Article

Self-Supporting g-C$_3$N$_4$ Nanosheets/Ag Nanoparticles Embedded onto Polyester Fabric as "Dip-Catalyst" for Synergic 4-Nitrophenol Hydrogenation

Abdallah Amedlous [1],* , **Mohammed Majdoub [1],*** , **Zakaria Anfar [2]** and **Elhassan Amaterz [2]**

[1] Laboratory of Materials, Catalysis & Valorization of Natural Resources, Hassan II University, Casablanca 20000, Morocco
[2] Laboratory of Materials & Environment, Ibn Zohr University, Agadir 80000, Morocco; zakaria.anfar@gmail.com (Z.A.); elhassan.amaterz@cnrs-orleans.fr (E.A.)
*   Correspondence: abdallah.amedlous@ensicaen.fr (A.A.); simajdoub@gmail.com (M.M.)

Abstract: Herein, we report the design of a cost-effective catalyst with excellent recyclability, simple recuperation and facile recovery, and the examination between the reaction cycles via the development of self-supporting g-C$_3$N$_4$ nanosheets/Ag NPs polyester fabric (PES) using a simple, facile and efficient approach. PES fabrics were coated via a sono-coating method with carbon nitride nanosheets (GCNN) along with an in situ setting of Ag nanoparticles on PES coated GCNN surface producing PES-GCNN/Ag^0. The elaborated textile-based materials were fully characterized using FTIR, ^{13}C NMR, XRD, TGA, SEM, EDX, etc. Catalytic performance of the designed "Dip-Catalyst" demonstrated that the as-prepared PES-GCCN/Ag^0 has effectively catalyzed the hydrogenation of 4-nitrophenol (4-NP) to 4-aminophenol (4-AP) in the presence of NaBH4. The 3×3 cm^2 PES-GCNN/Ag^0 showed the best catalytic activity, displaying an apparent rate constant (Kapp) equal to 0.43 min^{-1} and more than 10 reusability cycles, suggesting that the prepared catalyst-based PES fabric can be a strong nominee for sustainable chemical catalysis. Moreover, the coated fabrics exhibited appreciable antibacterial capacity against *Staphylococcus epidermidis* (*S. epidermidis*) and *Escherichia coli* (*E. coli*). The present study opens up new opportunities for the future design of a low cost and large-scale process of functional fabrics.

Keywords: PES fabrics; graphitic carbon nitride; Ag nanoparticles; 4-nitrophenol hydrogenation; dip-catalyst

1. Introduction

Nitro-aromatic compounds are considered one of the most frequent and stubborn organic pollutants found in industrial wastewaters due to their wide applications in several industries, such as pigments, dyes, plastics, pharmaceuticals, pesticides and fungicides [1]. Among them, 4-nitrophenol (4-NP) has been classified as a major pollutant by the US Environmental Protection Agency (EPA), owing to its potential toxicity toward human beings, fauna and flora [2]. On the contrary, 4-aminophenol (4-AP) (4-NP reductive derivative) is a valuable intermediate product used in the fabrication of paracetamol, clofibrate drugs, antioxygens and petroleum mixtures [3–5]. Therefore, it is highly important to adopt a sustainable clean route for treating such compounds in aqueous medium. In this regard, catalytic hydrogenation of 4-nitrophenol into 4-aminophenol has been the focus of several studies during the recent years [6–8].

Noble metal nanoparticles (NMNPs) have gained tremendous interests due to their fascinating physicochemical properties that are generally superior to those of the bulk species [9,10]. Outstandingly, silver nanoparticles (Ag NPs) have drawn a great interest from the scientific community owing to their distinctive qualities, including antibacterial traits, relatively low cost and high catalytic activity [11,12]. By controlling factors such as

dispersion and size of the nanoscale metallic silver, various silver nanoparticle-based catalysts having multiple features have been developed [13–15]. However, silver nanoparticles suffer from some shortcomings, mostly associated to their toxicity, leading to environmental contamination, depletion of rare resources and health issues. Additionally, silver nanoparticles tend to form colloidal agglomerate throughout the catalytic operation, giving rise to unavoidable reduction in the catalyst active surface area leading to a decay of the catalytic behavior in an undergoing procedure [16]. To overcome these limitations, immobilization and stabilization of metallic nanoparticles onto high surface area inert matrices (support) has been demonstrated to be a potent method to prevent agglomeration [17–19].

Encapsulating metal nanoparticles on inert matrices has recently shown promise in preserving intrinsic properties and ensuring longevity of chemical stability, as well as achieving unique collective properties and uses by combining the features of separate components. Textile materials have emerged as an intriguing new class of supports owing to their many benefits, such as environmental sustainability, good flexibility, lightweight, high porosity and relatively low cost. During the last decade, functional polyester fabrics with distinctive properties, such as self-cleaning, UV absorption, antimicrobial and photocatalytic activities, have been prepared through immobilization of nanomaterials [20–25]. The key parameters for achieving high performance polyester materials are the compatibility and the stability of metal nanoparticles on polyester's surface. The interfacial interactions and the dispersion of metal nanoparticles on polyester's surface are two crucial factors to achieve high performance textile materials. Therefore, homogenous and stable dispersion of nanoparticles is very well desired to prevent the aggregation causing uneven distribution of metal nanoparticles on polyester's surface due to the poor wettability and lack of functional groups [26]. Various types of surface modification approaches have been used to improve polyester properties such as UV irradiation, plasma treatment, ozone oxidation hydrolysis and aminolysis [27,28]. However, the majority of these methods are time and energy consuming and tend to use highly toxic chemicals. To overcome these issues, methods of dip coating with various materials are proposed to be an alternative approach due to their high adhesion, high functionality, reproducibility and suitability to prepare on a large scale. Among them, atomically 2D thin-layered structures, such as graphene and its derivatives [29], graphitic carbon nitride nanosheets (GCNN), hexagonal boron-nitride (h-BN) and transition-metal dichalcogenides (TMDCs), are emerging as fascinating materials for a wide range of applications due to their unique physical properties. In particular, graphite-like carbon nitride nanosheets (GCNN) have attracted a lot of scientific interest because of their high adsorption capacity, good electron conductivity, large specific surface area, thermal stability and acid–alkali chemical resistance [30–32]. Moreover, GCNN possess a well crystallized lamellar structure that can promote charge transfer [33] and exhibit many π–π conjugations on the surface due to its nature as a π–conjugated 2D material. Besides, GCNN can be easily loaded by other materials because of their similarity with soft polymers [34,35]. For the prior reasons, GCNN are an ideal material for coating PES fabric, which can enhance the compatibility and the adhesion of Ag NPs on the PES surface; therefore, a superior catalytic activity can be achieved.

A part of our research strategy is devoted to the elaboration of multifunctional textile materials with enhanced physicochemical, catalytic and antibacterial properties for numerous applications, including catalytic conversion toward water decontamination. The present study has been conducted to extend the implementation scope of g-C_3N_4 nanosheets as 2D modifiers for the modification of textile fabric surface. More specifically, this work aims to confer new functionalities to the polyester fabric by incorporating a low fraction of g-C_3N_4 nanosheets followed by the deposition of compatible silver nanoparticles. Until now, very limited reports have dealt with the modification of textile materials for metal nanoparticles' incorporation. In fact, our group has dealt with the surface modification of polyester fabric by 2D MoS_2 nanosheets to enhance its compatibility and affinity with metal nanoparticles. The results showed that the MoS_2 nanosheets deposition has increased the adhesion properties of silver nanoparticles onto the textile fabric [36].

Inspired by those findings, two main subjects are of interest in this study. The first one is related to g-C$_3$N$_4$ as a novel 2D carbon-based modifier for the improvement of the adhesion properties of textile fabric. The second concern is related to the investigation of the influence of the deposition of silver nanoparticles on g-C$_3$N$_4$ coated PES fabric on the physicochemical, catalytic and antibacterial properties. To feature the two matters, we first described the operatory protocols to produce g-C$_3$N$_4$ nanosheets from urea alongside its full structural, morphological and thermal characterizations. Then, we incorporated g-C$_3$N$_4$ nanosheets into the PES fabric and, afterwards, the Ag nanoparticles were in situ generation via sono-chemical method producing PES-GCNN/Ag^0 fabrics with different Ag^0 loadings. The produced coated fabrics were fully characterized by means of several physicochemical characterizations, including XRD, FTIR, SEM/EDX and TGA. Furthermore, the catalytic performance and antibacterial activity of the produced "Dip-Catalyst" toward 4-NP hydrogenation were investigated in detail. The obtained findings open up new opportunities for the future design of the low cost and large-scale process of functional fabrics with promising catalytic and antibacterial properties.

2. Results and Discussion

2.1. Characterization of Graphitic Carbon Nitride (GCN)

The transformation of urea into graphitic carbon nitride nanosheets (GCNN) was conducted via thermal treatment and was confirmed by FTIR, XRD, TGA and ^{13}C NMR, as shown in Figure 1.
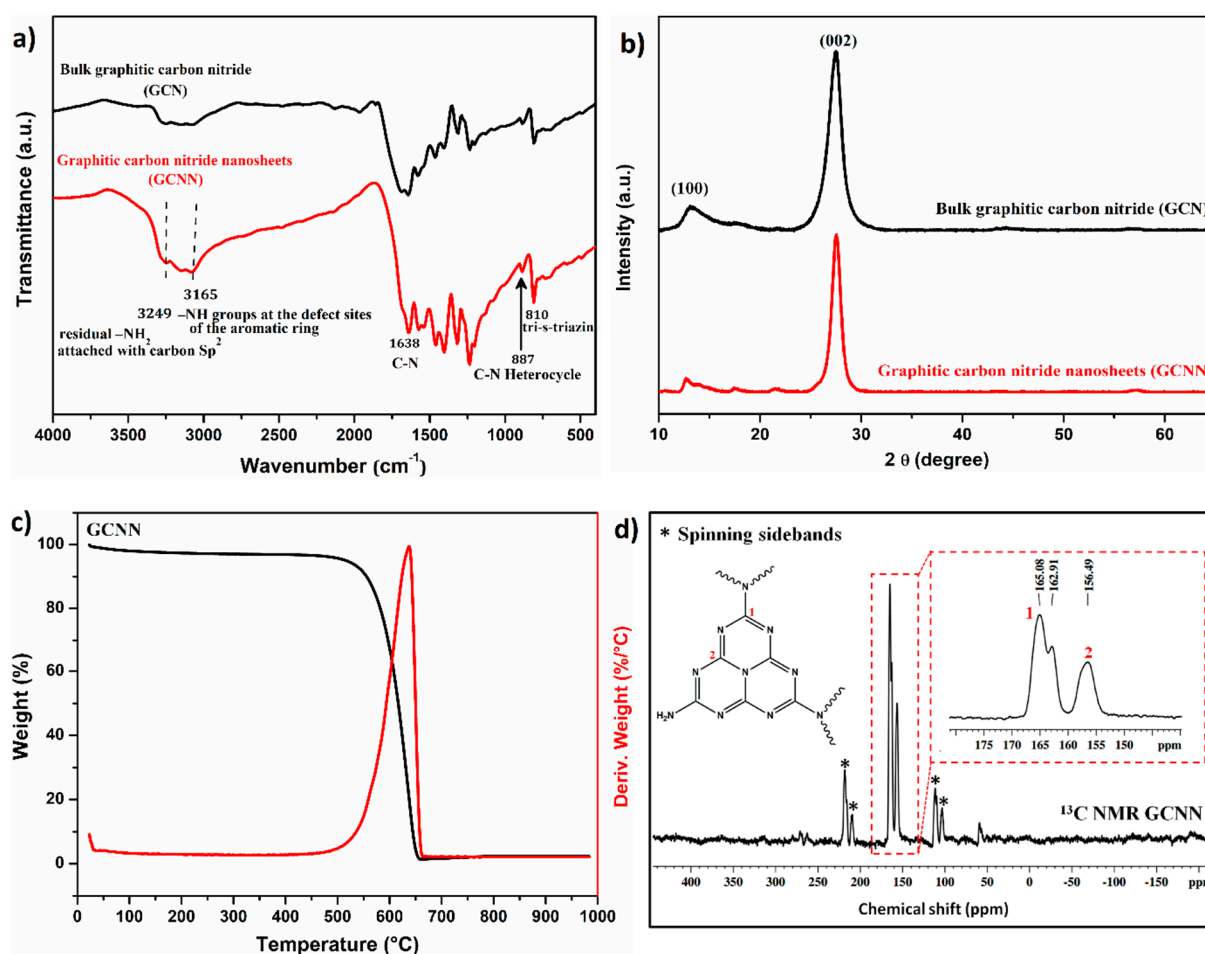
Figure 1. (**a**) FTIR of bulk and exfoliated GCN, (**b**) XRD diffractograms of bulk and exfoliated GCN, (**c**) TGA curve of GCNN, (**d**) ^{13}C MAS NMR of GCNN and ''*'' is the spinning sidebands.

Figure 1a displays the FTIR spectra of bulk and exfoliated GCN to further demonstrate their graphitic structures. Both samples exhibited quite similar absorption bands in terms of shape and position but with different intensities. The peaks intensities of exfoliated GCN slightly increased with respect to that of bulk GCN, indicating that the sono-exfoliation process has successfully occurred. The absorption bands located at 810 and 887 cm^{-1} were attributed to the deformation mode of the N–H bond resulting from the incomplete condensation of amino groups and the typical breathing mode of tri-s-triazine units, while the absorption bands at the region of 1200 to 1700 cm^{-1} were ascribed to the typical skeletal stretching modes of s-triazine derivatives, such as bridging C–NH–C or trigonal $(N-(C)_3)$ units (heterocyclic C–N) [37,38]. Both exfoliated and bulk GCN FTIR spectra displayed a broad absorption band at 3000–3500 cm^{-1} corresponding to the adsorbed H_2O molecules and N–H vibrations of the uncondensed amine groups [39].

X-ray diffraction was used to determine the crystal structure of both bulk and exfoliated GCN (XRD). The layer-to-layer distance of GCN materials was also determined using this method. As shown in Figure 1b, two peaks at 13.2° and 27.7° in both samples' XRD patterns could be properly indexed. The diffraction peak at 13.2° (0.67 nm) corresponded to the in-planar structural packing motif, whereas the 27.7° peak (0.32 nm) is attributed to the usual layer-by-layer stacking of the conjugated aromatic groups [40]. It is worth mentioning that the exfoliated GCN exhibited a significant decrease in both peaks at 27.7° (002) and 13.2° (100), which suggest that the exfoliation process via ultrasonication has successfully occurred since GCNN were generated via the exfoliation of bulk GCN. Nevertheless, the peak positions remained constant which indicates that the layered GCN structure remains in the exfoliated GCNN, keeping the interlayer distance constant [41].

Thermogravimetric analysis (TGA) was utilized to assess the synthesized material's thermal stability. As can be seen from Figure 1c, at temperatures between 500 and 700 °C, the GCNN sample showed a rapid and uniform weight loss, corresponding to the thermal breakdown of the carbon nitride backbone into nitrogen and carbon-containing gaseous species.

The ^{13}C cross-polarization magical angle spinning (^{13}C CP-MAS) solid state NMR analysis was also carried out to assist in the structural elucidation of the GCNN sample, with the result being shown in Figure 1d. According to this figure, the ^{13}C MAS NMR of the GCNN sample prepared via thermal treatment exhibited two apparent and typical resonance groups: the first resonance groups at 163.0 and 165.1 ppm were attributed to the carbon atoms (C_1) connected with –NH_2 groups, also called $CN_2(NH_2)$ groups, whereas the other resonance at 156 ppm was associated with the carbon species in heptazine units and linked with bridging N atoms(C_2), also referred as CN_3 groups of the cyameluric nucleus. These assignments are in good accordance with those reported of graphitic carbon nitride [42–44], further indicating the prepared GCNN were mainly consisting of heptazine tectonic units.

The morphologies of the as-prepared GCNN sample were examined by scanning electron microscopy (SEM). From Figure 2a,b, it is clearly seen that GCNN were composed of irregular and lamellar folded-like wrinkled sheets, where the layers stacking can be observed. TEM observations were performed to have more insights about the layer–layer morphology of the elaborated GCCNN material. According to Figure 2c,d, the elaborated GCNN consisted principally of multilayer edgeways nanosheets, forging a well-defined 2D morphology. In addition, GCNN were distinguished by the presence of small size characteristic folds and creases, indicating the attainment of a high exfoliation degree using ultrasonication treatment. Furthermore, the examinations demonstrated that the GCNN specimen consists majorly of piled small size nanosheets with a relatively translucent, fluffy and rippled aspect.
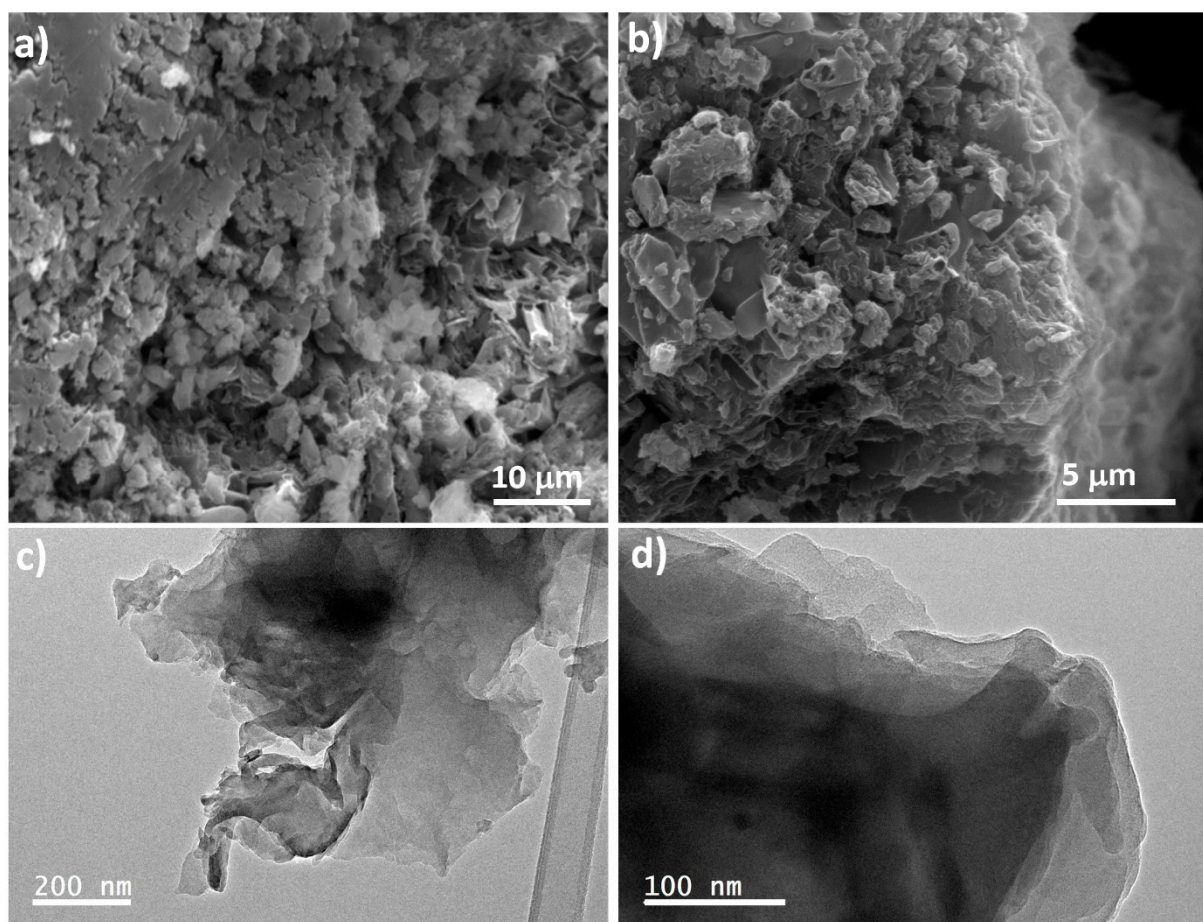
Figure 2. (**a**,**b**) SEM and TEM and (**c**,**d**) images of the prepared GCNN.

2.2. Characterization of PES Based Materials

ATR-FTIR spectroscopy was used to examine the chemical structure of non treated and coated PES based catalyst, respectively. By using FTIR, the potential interfacial interactions occurring between PES, GCNN/Ag^0 coatings were identified. Figure 3 shows typical ATR-FTIR spectra of neat PES, PES-GCNN and PES-GCNN/Ag^0 10 textiles, as well as PES-GCNN/Ag^0 fabrics.

As can be seen from this figure, the FTIR spectra of all the fabric based samples exhibited the essential absorption bands of polyester functional moieties, particularly the presence of the following absorption bands: 1712 cm^{-1} (C=O stretching of aromatic ester), 1250 cm^{-1} (aliphatic ester C=O stretching vibration), 1018 cm^{-1} (in-plane vibration of benzene), 1095 cm^{-1} (ester C=O stretching), 972 cm^{-1} (C–O stretching of glycol) and 725 cm^{-1} (out of plane benzene ring group) [45,46]. The FTIR spectra of the PES-GCNN sample exhibited some remarkable differences, counting a well noticed decrease in the carbonyl stretching vibrations' intensity (1712 and 1250 cm^{-1}). This indicates that GCNN established strong interfacial interactions with the PES fibers, which may occur between the aromatic/aliphatic ester moieties of PES and N–H/C–N groups of the heptazine units in GCNN backbone, or through π–π interactions between the benzene rings of PES fabric and s-triazine derivatives, thus giving rise to a homogeneous GCNN coating on PES surface. Moreover, the emergence of new peaks at 3249 and 3165 cm^{-1} in the FTIR spectra of PES/GCNN corresponding to the N–H vibrations of the uncondensed amine groups of GCNN gave additional supports to the establishment of strong interactions between the PES and GCNN.

In comparison with the PES-GCNN sample, the PES-GCNN/Ag^0 10 fabric showed no noteworthy changes with the absence of silver nanoparticles vibrational bands which were

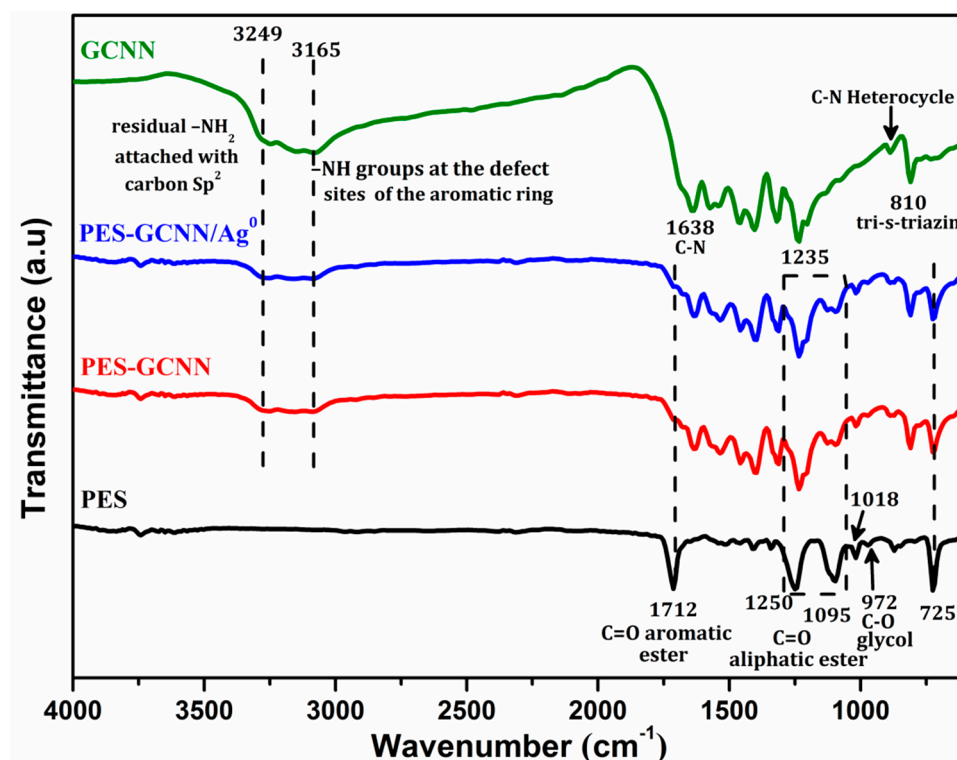overwhelmed by the PES-GCNN fabric owing to the low loading of Ag nanoparticles on the sample's surface.

Figure 3. FTIR spectra of PES, PES-GCNN, PES-GCNN/Ag^0 10 and GCNN.

X-ray diffraction (XRD) was used to determine the crystalline phase of uncoated PES, PES-GCCN and PES-GCCN/Ag^0 samples (Figure 4). According to this figure, the XRD diffractogram of unmodified PES revealed the emergence of three broad diffraction peaks at 2-theta = 17.51°, 22.71° and 25.61°, indicating the existence of crystal regions allocated to the PES crystalline phase/hard segment (semi-crystalline PES) (Lu et al. 2011). The PES-GCNN fabric did not exhibit any apparent extra peaks associated with GCNN, indicating that the GCNN coating had no effect on the crystallinity of neat PES. After conducting an in-situ reduction of Ag$^+$ to Ag NPs (Ag^0) onto PES-GCNN, the XRD patterns of PES-GCCN/Ag^0 10 revealed the emergence of four prominent peaks at 2-theta = 37.47°, 43.69°, 63.97° and 77.02°, which were assigned to the cubic Ag^0 planes (111), (200), (220) and (311), respectively. The Debye–Scherrer equation was used to determine the average crystallite size, which was 13.3 nm.

The thermal degradation profile of unmodified and modified PES based catalysts was examined using TGA under air flux with 10 °C min^{-1} rate. The thermograms of all samples are shown in Figure 5, and the parameters derived from them are given in Table 1. As can be seen from Figure 5, it is clearly noticeable that all coated fabrics, regardless of coating nature, principally undertake two recognizable decomposition stages. (1) A first decomposition stage occurs between 300 and 496 °C, assigned to the thermal decomposition of ester bond in the polyester sample, which arises from the chain scission based depolymerization along the polyester giving rise to vinyl- and carboxy-ended chain fragments that produce volatile cyclic oligomers. (2) The subsequent thermal degradation step occurs at up to 610 °C, which is attributed to the cleavage of carbon–carbon linkage, giving rise to the generation of volatile gazes including CO, CO$_2$, CH$_4$, benzene, ethylene, etc. [47]. In comparison with pristine PES, the PES-GCNN and PES-GCNN/Ag^0 10 fabrics showed improved thermal stability, which can be assigned to the strong non-covalent interactions settled between the GCNN and GCNN/Ag^0 coatings and the PES fabric. For instance, coating PES fabric with GCNN and GCNN/Ag^0 resulted in an increase in the

thermal decomposition temperature at maximum rate (T_{dmax}) for the first degradation stage from 419.1 to 439.3 (Table 1). Generally, the thermal degradation of the coated samples occured at an elevated temperature compared to neat PES. The consequential increase in T_{di} (300.1 °C for PES vs. 308.6 °C for PES-GCNN and 315.5 for PES-GCNN/Ag^0 10) and T_{dm} (489.1 °C for PES vs. 463.2 °C for PES-GCNN) for the first stage of thermal decomposition gave further proof that GCNN and GCNN/Ag^0 coatings has strongly boosted the general thermal decompostion resistance of PES specimens. However, it is clearly noticeable that the PES-GCNN/Ag^0 TGA curve exhibited a rapid second thermal degradation stage, i.e., cleavage of the C–C bond, in comparison with pristine PES and PES-GCNN, which can be ascribed to the catalyzing effect of Ag^0 over the C–C scission in the PES-GCNN thermal degradation [48]. Further information worth mentioning is that the residual weight fraction of PES-GCNN/Ag^0 was found to be approximetly 10 wt%, which is considered to be the content of Ag nanoparticles in the PES-GCNN/Ag^0 10 fabric.
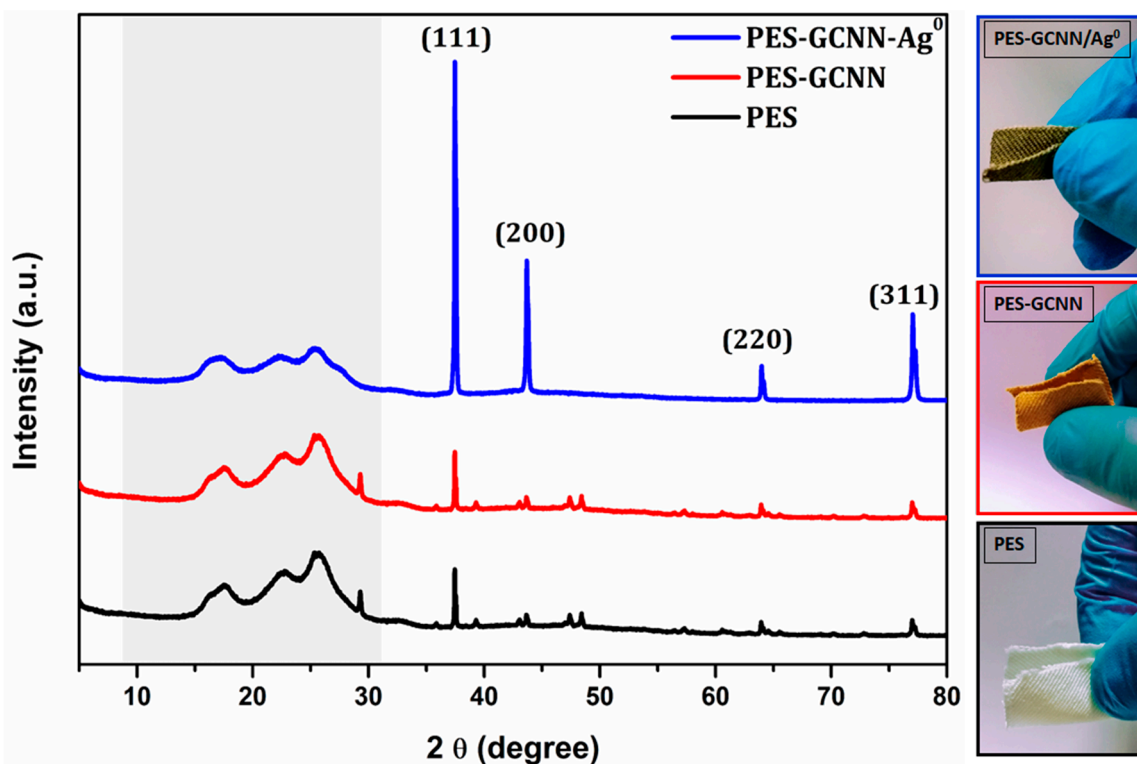

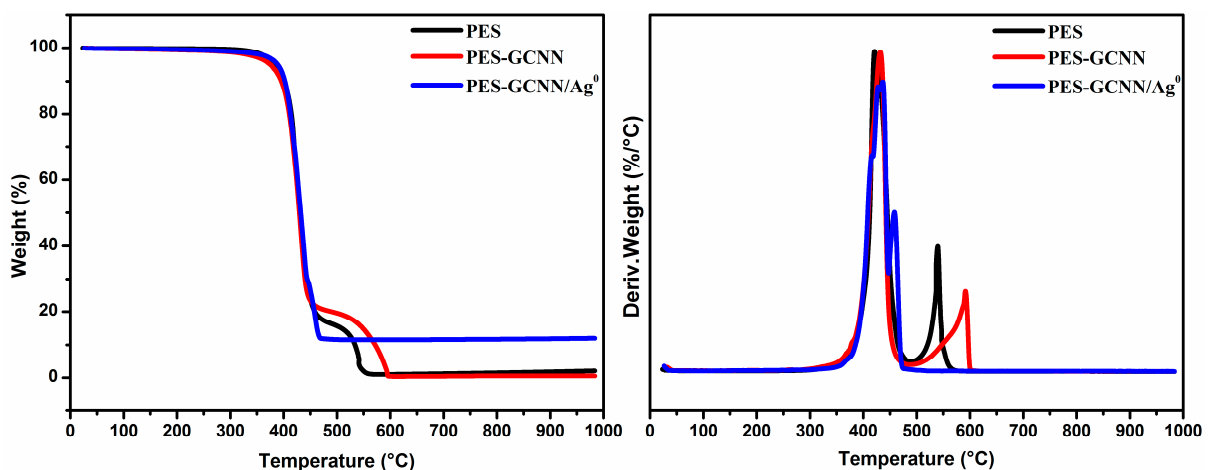**Figure 4.** XRD patterns of uncoated PES fabric, PES-GCNN and PES-GCNN/Ag^0 10.

Figure 5. TGA and DTG thermogarms of PES, PES-GCNN, PES-GCNN/Ag^0 10.

**Table 1.** Thermal parameters of decomposition stages of the fabric-based samples.

Sample Code	Stage 1: Ester Linkage Decomposition		Stage 2: C–C Cleavage (Oxidation)	
	T_{di}–T_{df} (°C)	T_{dmax} (°C)	T_{di}–T_{df} (°C)	T_{dmax} (°C)
PES	300.1–489.1	419.2	498.5–579.4	540.2
PES-GCNN	308.6–496.4	431.1	501.7–606.7	590.9
PES-GCNN/Ag^{0}10	315.5–448.3	439.3	449.9–495.2	458.4

T_{di}: The initial thermal degradation temperature. T_{df}: The final thermal degradation temperature. T_{dmax}: The thermal degradation temperature at maximum rate.

SEM examinations were conducted to investigate the morphology of the textile-based catalyst and GCNN/Ag^0 degree of dispersion onto the PES surface. SEM micrographs of textile-based catalysts are given in Figure 6. Pristine PES exhibited a well ordered surface, which is composed of extended, intertwisted and knotted microfibers. SEM micrographs of the elaborated PES-GCNN sample clearly displayed a complete change in the surface morphology, going from a microsmooth morphology for pristine PES (Figure 6a,d) to a microrough morphology for PES-GCNN (Figure 6b,e), owing to the dip-coating process via ultrasonication that grants a full wrapping of PES microfibers with GCNN, thus improving the adhesion characteristics. Following the depostion of silver nanoparticles on the PES-GCNN surface via in situ reduction, SEM micrographs of PES-GCNN/Ag^0 10 (Figure 6c,f) revealed similar roughnesss to that of the PES-GCNN sample, accompanied with the appearance of deposited silver nanoparticle (Ag^0) onto its surface. The in situ deposited Ag^0 mainly consisted of homogeneous and uniform quasi-spherical nanoparticles with no sign of aggregation (inset of Figure 6f). Herein, the preceding GCNN coating on the PES surface had the capability to enhance the compatibility and adhesion properties of PES fibers, thus allowing the homogeneous capture and deposition of Ag nanoparticles.

In order to confirm the uniformity of Ag NPs distribution, EDX mapping was carried out under SEM examinations. The EDX result, as given in Figure 7, in addition to elemental mapping images, demonstrated that the produced PES-GCNN/Ag^0 10 fabric was comprised of C, O, N and Ag elements. The mapping images also demonstrated a relatively homogeneous and uniform Ag element distribution in the fabric sample, which implied that Ag NPs were uniformly anchored on the PES-GCNN/Ag^0 10 surface.
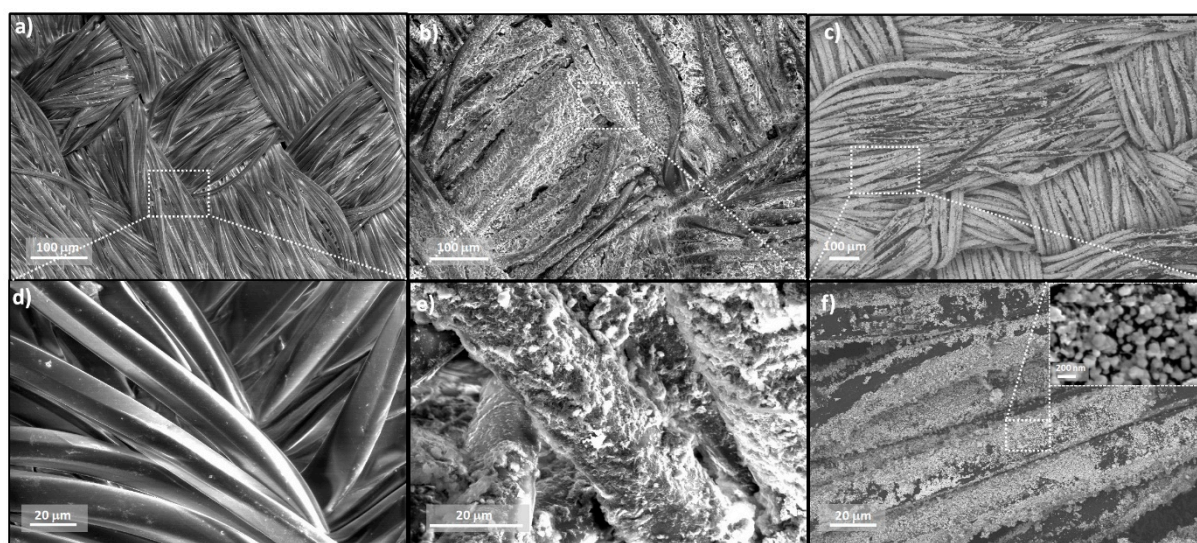
Figure 6. SEM micrographs of (**a**,**d**) PES, (**b**,**e**) PES-GCNN and (**c**,**f**) PES-GCNN/Ag^0 10.
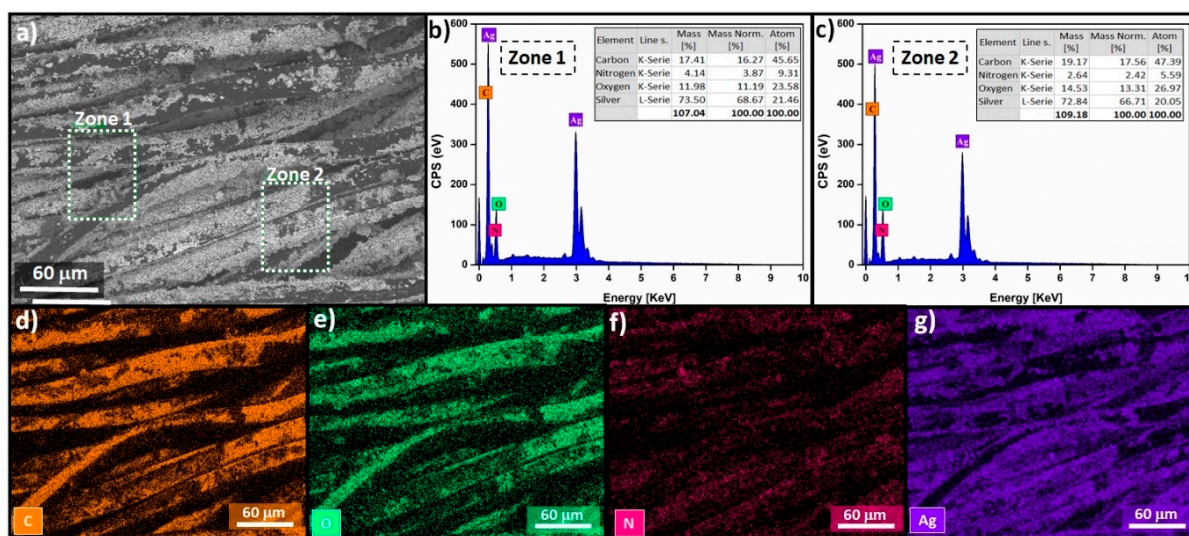
Figure 7. The energy dispersive X-ray (EDX) mapping analysis of the PES-GCNN/Ag^0 10 fabric. (**a**) The explanation for subfigure is EDX Mapping, (**b**,**c**) the EDX spectrum of the PES-GCNN/Ag^0 in two zones, and the EDX-mapping distribution of carbon (**d**), oxygen (**e**), nitrogen (**f**) and silver nanoparticles (**g**).

To test how well the deposited Ag nanoparticles adhered to PES-GCNN fabric, we immersed different substrates, including PES-GCNN, PES-GCNN/Ag^{0}10 and PES-Ag^0 as a reference fabric, in ethanol solution. Afterwards, the samples were rapidly stirred at 500 rpm for 24 h. A total of 3 mL of the reaction mixture was collected at 1 min intervals throughout the experiment. The excellent adherence of Ag nanoparticles on the PES-coated GCNN differs markedly from the samples that lacked the GCNN where the deposited Ag easily slid off the surface by simple shaking, as displayed by the weight change in Table 2.

Table 2. Comparison of mass change of each sample after the adhesion test.

Sample	$m/m_{0(t=0)}$	$m/m_{0(t=24h)}$
PES-GCNN	1	1
PES-GCNN/Ag^0 10	1	0.99
PES-Ag^0 (reference)	1	0.48

2.3. Antibacterial Activity and Antibacterial Adhesion

As can be seen from Figure S1, neat PES and PES-GCNN fabrics did not show any antibacterial activity. In contrast, silver nanoparticles-filled PES-GCNN fabric (PES-GCNN/Ag^0) displayed a relatively significant bactericidal efficiency to both Staphylococcus aureus and *Escherichia coli*. In the case of Staphylococcus aureus, the PES-GCNN/Ag^0 sample displayed an inhibition zone up to 3 mm (Figure S1a), while it revealed an inhibition zone of 4 mm for *Escherichia coli* (Figure S1c). The bactericidal mechanism of silver nanoparticles is not fully understood in the state of the art. The most accepted one consists of the release of Ag$^+$ ions by silver nanoparticles, affecting the metabolic processes and the mechanism of cell division, resulting in serious problems in the membrane permeability, thus the death of the bacteria [49,50].

Figure S1b,d shows the adhesion of both Staphylococcus aureus and *Escherichia coli* on the surface of PES based samples. There were no bacterial colonies around and under PES-GCNN/Ag^0 round pieces after the incubating time. In contrast, some bacterial colonies grew around and under the neat PES and PES-GCNN fabrics. This phenomenon was observed in Staphylococcus aureus and *Escherichia coli*. Hence, the PES-GCNN/Ag^0 fabric exhibited significant improvement in the property of antibacterial adhesion. These findings demonstrated that the produced PES-GCNN/Ag^0 fabrics an appropriate candidate

in a variety of industrial applications that require materials with long term antibacterial and anti-adhesion properties.

2.4. Catalytic Hydrogenation of 4-Nitrophenol over PES-GCNN/Ag^0

To evaluate the catalytic performance of various as-prepared PES-GCNN/Ag^0 catalysts, reduction of 4-NP to 4-AP in the presence of excess $NaBH_4$ was chosen as a model reaction. As it is well known, the light-yellow 4-NP aqueous solution (0.03 mM) exhibits an absorption peak at around 318 nm. After addition of $NaBH_4$ (0.1 M), the color of the solution changes into greenish yellow and the maximum of this peak shifted to 400 nm due to the formation of 4-nitorphenolate ions (Figure 8a,e).

The changes related to the concentration (C_t/C_0) of 4-nitorphenolate as a function of reaction time using a series of Ag^0-containing catalysts is shown in Figure 8c,d. It should be noted that no conversion of 4-NP to 4-AP was obtained after 3 days in the absence of a catalyst. In addition, it can be seen from the obtained result that PES-GCNN is inactive for reduction of 4-nitorphenolate. In contrast, the addition of different amounts of Ag^0, the catalytic activity of PES-GCNN/Ag^0 samples gradually elevated with the increased amount of Ag NPs. This may suggest that Ag^0 NPs can facilitate electron transfer from BH_4^- to 4-nitrophenolate, and thus lowers down the barrier of activation energy for reducing 4-NP to 4-AP.

The reaction using the PES-GCNN/Ag^0 10 catalyst showed the best catalytic activity. Figure 8b shows ultraviolet–visible spectra for successive reduction of 4–NP with $NaBH_4$ using the PES/GCNN-Ag^0 10 catalyst. When the PES/GCNN-Ag^0 10 catalyst is introduced into the solution, the absorption peak at 400 nm decreases with the time of reaction; in contrast, a new peak appears at λ_{max} = 300 nm attributed to 4-AP and its intensity simultaneously elevates. It is worth mentioning that increasing the loaded amount of Ag NPs increased the reaction rate. For instance, the conversion of 4-NP displayed 90% after 5 min of reaction time using the PES/GCNN-Ag^0 10 sample, with apparent rate constant (Kapp) up to 0.462 min^{-1} (Figure 8d).

It was assumed that the surface porosity of fabric provides high sorption of both acceptor (4-NP) and donor (BH_4^-) species, which enhanced the rate of reduction by increasing electron transfer between the reacting substances [51]. This assumption was further reinforced by studying the effect of the surface of PES fabric coated with GCNN/Ag^0 NPs on the 4-NP reduction process. Accordingly, we performed experiments varying the surface of catalyst (0.25, 1, 4 and 9 cm^2), while reaction parameters such as concentration of 4-NP and $NaBH_4$ were kept constant. Conversion profiles of the different surface of the catalyst are shown in Figure 9a. The rate constants for 0.25, 1, 4 and 9 cm^2 are 0.032, 0.098, 0.154 and 0.462 min^{-1}, respectively (Figure 9b). It was observed that the rate constant increased gradually with the increase in the surface of catalyst. The result means that: (1) the increase in the surface of the catalyst, the more active sites are generated, (2) a higher availability of surface for the adsorption of reacting species and (3) homogenous coating was obtained.
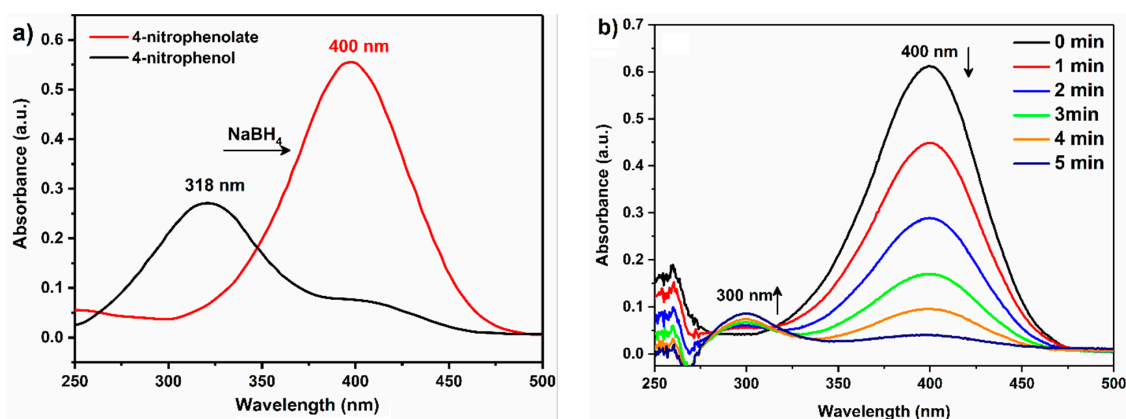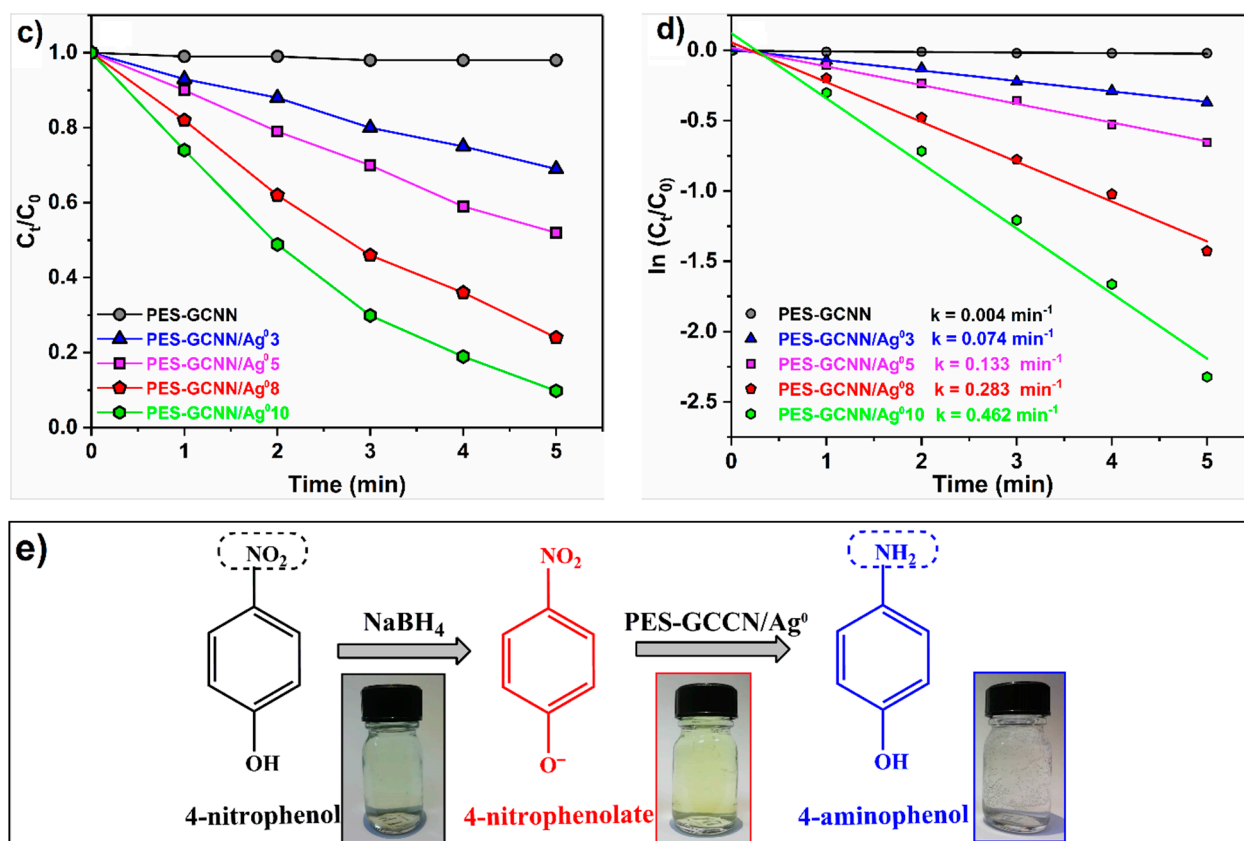

Figure 8. *Cont*.

Figure 8. (**a**) UV–vis of control spectra obtained before (4-NP) and immediately after addition of NaBH$_4$. (**b**) A series of absorbance spectra obtained every 1 min after addition of the PES-GCNN/Ag^{0}10 catalyst [3 × 3 cm^2] to a solution containing 4-NP and NaBH$_4$. (**c**) Time-dependent 4-NP conversion over various Ag^0 containing catalysts and (**d**) the corresponding kinetics plots. (**e**) Reaction scheme and photographs representing reduction of 4-NP to 4-AP by NaBH$_4$, catalyzed by PES-GCNN/Ag^0.
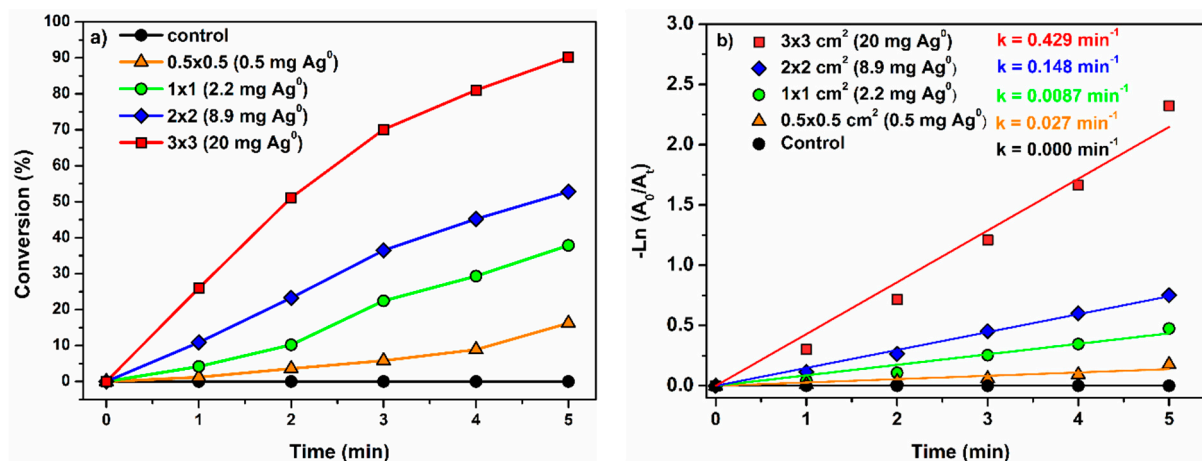

Figure 9. Comparison of catalytic activity of different area of PES-GCNN/Ag^0 catalyst fabric. (**a**) Conversion profiles for the 4-NP. (**b**) Plot of ln(C/C$_0$) against the reaction time for the reduction of 4-NP by NaBH$_4$ using different area of PES-GCNN/Ag^0 catalyst fabric.

2.5. Recyclability and Stability of Catalyst

The recyclability and stability of the catalyst are the most important parameters of its application as a heterogeneous catalyst. As shown in Figure 10, the PES-GCNN/Ag^{0}10 catalyst can be reused for ten cycles in succession without significant reduction in its

catalytic activity. In order to verify whether soluble catalytic species play a role in 4-NP reduction reaction, the PES-GCNN/Ag^0 fabric is removed after 3 min of reaction and the filtrate obtained was stirred for an additional 30 min. Conversion percentage of 4-NP in the presence of the catalyst after 2 min of reaction showed 51%, while no increase in conversion of 4-NP was obtained in the catalyst-free. This result demonstrates that our catalyst was responsible for the reaction, and clearly rules out the possibility of leached Ag catalyzing the reaction. The catalytic and structural stability of PES-GCNN/Ag^0 could be expected as a promising catalyst for the industrial production.
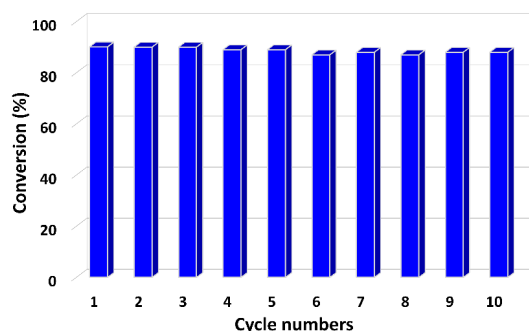

Figure 10. Cycling performance of PES-GCNN/Ag^0 for 4-NP reduction reaction conditions.

The 4-NP conversion over PES-GCNN/Ag^0 NPs was compared with some other catalysts previously reported at different reaction conditions (concentrations of 4-NP, catalyst loading and reaction time), as summarized in Table 3. From this comparison data, we can clearly show that our catalyst exhibited an enhanced catalytic activity for 4-NP conversion, which is comparable and noticeably higher than previous reported silver-based catalysts.

2.6. Mechanism of 4-NP Reduction Reaction by PES-GCNN/Ag^0

By adopting Langmuir–Hinshelwood model, it is possible to describe how the reduction mechanism of the reaction occurs when both reactants (BH$_4$$^-$ and 4-NP) are adsorbed on the surface and inside PES pores in distinct catalytic active sites [58,59]. Figure 11 depicts a possible 4-NP catalytic hydrogenation route utilizing the PES-GCNN/Ag^0 catalyst in NaBH$_4$ presence. The BH$_4$$^-$ ions react with the active surface of metallic Ag^0 nanoparticles in reaction medium to generate active hydrogen species. This reaction occurs first in aqueous solution. Meanwhile, the generated 4-nitrophenolate ions present in the solution migrate into pores between the PES fibers, where they proceed to a reaction with active hydrogen-containing species, thus producing 4-hydroxylaminophenol as a stable intermediate that is eventually transformed to 4-aminophenol.
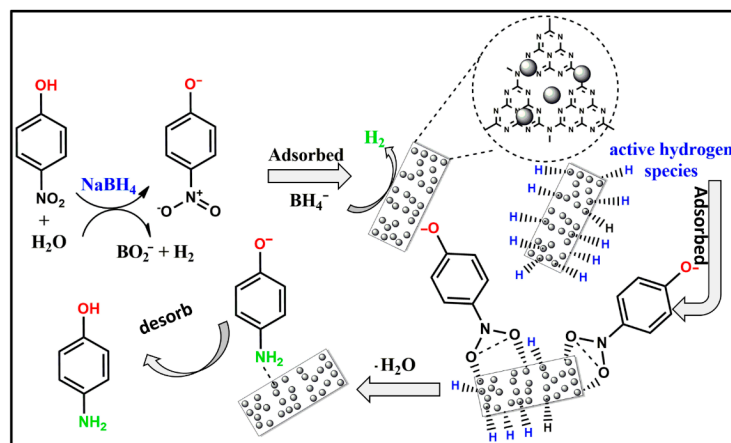
Figure 11. Possible 4-NP catalytic reduction route by NaBH$_4$ over PES-GCNN/Ag^0.

Table 3. Comparison of the activity of our catalysts with other reported catalysts for 4-NP to 4-AP.

Catalyst	Support	4-NP (mM)	k_{app} (min^{-1})	Quantity of Catalyst Used (mg)	Reaction Time (min)	Conve-rsion %	Ref.
Ag NPs	None	5	0.19	2.7	20	100	[52]
$_R$GO/Ag	Graphene oxide	0.2	0.216	1	15	100	[53]
$_R$N–GO/Ag	N-doped graphene oxide	0.2	0.444	1	6.6	100	[53]
Ag/MoS$_2$	MoS2	0.1	0.29	1.5	12	94.5	[54]
SiO$_2$/Ag	SiO$_2$	0.12	0.213	15	10	78	[55]
Fe$_3$O$_4$@SiO$_2$–Ag	Fe$_3$O$_4$@SiO$_2$	5	0.83	3	4	96	[56]
Ag/C	Carbon	0.12	0.32	2	12	98	[8]
Ag/PANI	Polyaniline	5	1.28	2.7	3	100	[52]
g-C$_3$N$_4$/Ag$_2$S	Graphitic carbon nitride	2.5	0.0311	0.0008 (10 mg/L)	42	97	[57]
PES-GCNN/Ag^0	PES-GCNN	0.03	0.462	20 [a]	5	90	This study

[a] Not including PES weight.

3. Experimental Section

3.1. Materials and Chemicals

A local Fez manufacturer supplied the polyester fabric (90 g/m^2). 4-nitropheonol ($C_6H_5NO_3$) was provided by Merck, as was silver nitrate ($AgNO_3$, 99.9%), urea (CH_4N_2O), sodium borohydride ($NaBH_4$) and ammonia solution (28%). All the experiments were conducted with bi-distilled water.

3.2. Preparation of Graphitic Carbon Nitride Nanosheets (GCNN)

Graphitic carbon nitride nanosheets (GCNN) were synthesized on the basis of the procedures previously reported in the literature with some modifications [60]. Typically, urea (15 g) was put in a covered crucible and calcined under air atmosphere at 550 °C for 4 h with a ramping rate of 2.5 °C/min. The powder was collected and placed in an open crucible and further heated at 500 °C for 2 h with a ramp rate of 5 °C/min. Then, the obtained brownish powder was washed several times with distilled water to remove any residual alkaline species (i.e., ammonia) and further drying in a vacuum oven at 60 °C overnight. The obtained powder was re-dispersed in aqueous medium and then exfoliated via ultrasonication using Brandson Digital Sonifer (S450D, 35% amplitude) to generate graphitic carbon nitride nanosheets (GCNN). Finally, the product was centrifuged and washed with distilled water and dried at 60 °C overnight.

3.3. Preparation of Polyester Coated GCNN and GCNN/Ag NPs

The PES-GCNN fabric was sono-coated. First, polyester fabric samples (8 × 3 cm) were pretreated with 1 g/L aqueous ammonia and 1 g/L nonionic detergent for 30 min at 60 °C. The textiles were then washed with distilled water and dried in a vacuum oven at 60 °C for 2 h. Exfoliated GCNN aqueous solution (1 mg/mL) was applied to prepare PES/GCNN specimens by dip-coating under ultrasonication for 45 min, washed with water/ethanol mixture to detach residual GCNN, then dried at 70 °C for 2 h. After the GCNN coating, the color was obviously changed from white to brown.

The resulting PES-GCNN (5 wt% of GCNN) fabric was submerged in an aqueous solution of $AgNO_3$ (0.5 M) for 30 min before being subjected to an ultrasonication treatment at room temperature. Later, the sample was withdrawn from the $AgNO_3$ solution and put in $NaBH_4$ aqueous solution (1 M) for 30 min at ambient temperature, thus reducing the Ag^+ metallic ions to Ag^0 (Ag nanoparticles). Using distilled water, the PES-GCNN/Ag^0 samples with different Ag^0 wt% were cleaned to detach any non-reduced Ag^+. Finally, the samples were dried at 60 °C for 2 h.

3.4. Catalytic Hydrogenation of 4-Nitrophenol

In order to investigate the catalytic performance of the elaborated textile-based catalyst, a freshly prepared $NaBH_4$ aqueous solution (5 mL, 0.1 M) was added to a 4-NP solution (15 mL, 0.03 mM). Afterwards, PES-GCNN/Ag^0 catalyst in a squared form was introduced by simple immersion to the above mixture. To analyze UV–vis absorption spectra (6705 UV/vis JENWAY) throughout the 4-NP reduction process, 3 mL of the reaction mixture was collected at 1 min intervals throughout the experiment. Immediately after completion of the reaction, the PES-GCNN/Ag^0 fabric was removed from the reaction medium, washed with bi-distilled water and then dried to further examine its reusability.

3.5. Characterization Techniques

Infrared spectroscopy was used to investigate the chemical structure of the GCNN, and the textiles were generated using a Bruker Vector 22 instrument in transmission mode. The GCN and GCNN were softly crushed and pressed into KBr pellets for FTIR characterization. FTIR spectra were collected at 32 cm^{-1} resolution between 400 and 4000 cm^{-1}. All spectra were collected after 128 scans.

Cross-polarization magic angle spinning (CP-MAS) ^{13}C solid-state NMR spectra were recorded using the combined techniques of magic angle spinning (MAS) and cross

polarization (CP). Experiments were performed at room temperature in a Bruker Avance III-600 spectrometer equipped with a 4-mm MAS probe.

The phase purity and composition of the sample were determined by X-ray diffraction (XRD) using a Model: D8 Discover Bruker AXS with CuKα radiation (λCu = 1.5407) and a scan speed of $0.1°/\text{min}$.

TGA-Model Q500 (TA Instrument) was used to perform thermogravimetric analysis (TGA). The thermal stability was investigated by heating specimens of about 50 mg from 25 to 1000 degrees Celsius at a heating rate of 5 °C/min under air atmosphere with a flow rate of 90 mL/min^{-1}.

The transmission electron microscopy (TEM) was carried out using JEOL ARM200 imaging apparatus. A carbon grid was used to deposit the samples, which were then allowed to dry before being examined.

Scanning electron microscopy (SEM) (AFEI Quanta 200-ESEM) was used to examine the surface morphology of the produced materials, with an accelerating voltage of 40 kV.

The adhesion experiments of the manufactured textile-based catalysts were performed as described by Lee et al. [61]. Typically, 30 mm squared specimens were first dried at 70 °C for 24 h, then weighted (m_0) and stirred in ethanol solution at 500 rpm for 24 h. After stirring, the specimens were dried in air for 1 h, then vacuum dried at 80 °C overnight, and then weighed again (m) for the assessment of coating adherence.

4. Conclusions

In this study, we report a novel catalyst based on graphitic carbon nitride nanosheets (GCNN) coated on PES fabric and decorated with Ag NPs. The catalyst was prepared via dip-coating method followed by in situ reduction of Ag^+ to Ag^0 in its surface. Various physicochemical characterizations were used to study the possible interfacial interactions between PES, GCNN and $GCNN/Ag^0$. The resulting catalytic activity of PES-GCNN/Ag^0 on hydrogenation of 4-NP reaction showed the best catalytic activity and excellent recyclability with unchanged catalytic efficiency for more than 10 consecutive cycles. In addition, the results show that GCNN/Ag^0 coatings on PES substrate can be beneficial to overcome difficulties of separation of powder. This study demonstrated that the as-prepared PES-GCNN/Ag^0 can be a promising candidate for important organic conversions and industrial applications.

References

1. Herrera-Melián, J.A.; Martín-Rodríguez, A.J.; Ortega-Méndez, A.; Araña, J.; Doña-Rodríguez, J.M.; Pérez-Peña, J. Degradation and detoxification of 4-nitrophenol by advanced oxidation technologies and bench-scale constructed wetlands. *J. Environ. Manag.* **2012**, *105*, 53–60. [CrossRef]
2. Li, J.; Kuang, D.; Feng, Y.; Zhang, F.; Xu, Z.; Liu, M. A graphene oxide-based electrochemical sensor for sensitive determination of 4-nitrophenol. *J. Hazard. Mater.* **2012**, *201–202*, 250–259. [CrossRef] [PubMed]

3. Li, J.; Liu, C.Y.; Liu, Y. Au/graphene hydrogel: Synthesis, characterization and its use for catalytic reduction of 4-nitrophenol. *J. Mater. Chem.* **2012**, *22*, 8426–8430. [CrossRef]

4. Lv, J.J.; Wang, A.J.; Ma, X.; Xiang, R.Y.; Chen, J.R.; Feng, J.J. One-pot synthesis of porous Pt-Au nanodendrites supported on reduced graphene oxide nanosheets toward catalytic reduction of 4-nitrophenol. *J. Mater. Chem. A* **2015**, *3*, 290–296. [CrossRef]

5. Lu, S.; Yu, J.; Cheng, Y.; Wang, Q.; Barras, A.; Xu, W.; Szunerits, S.; Cornu, D.; Boukherroub, R. Preparation of silver nanoparticles/polydopamine functionalized polyacrylonitrile fiber paper and its catalytic activity for the reduction 4-nitrophenol. *Appl. Surf. Sci.* **2017**, *411*, 163–169. [CrossRef]

6. Chen, X.; Chen, X.; Cai, Z.; Oyama, M. AuPd bimetallic nanoparticles decorated on graphene nanosheets: Their green synthesis, growth mechanism and high catalytic ability in 4-nitrophenol reduction. *J. Mater. Chem. A* **2014**, *2*, 5668–5674. [CrossRef]

7. Layek, K.; Kantam, M.L.; Shirai, M.; Nishio-Hamane, D.; Sasaki, T.; Maheswaran, H. Gold nanoparticles stabilized on nanocrystalline magnesium oxide as an active catalyst for reduction of nitroarenes in aqueous medium at room temperature. *Green Chem.* **2012**, *14*, 3164–3174. [CrossRef]

8. Chi, Y.; Tu, J.; Wang, M.; Li, X.; Zhao, Z. One-pot synthesis of ordered mesoporous silver nanoparticle/carbon composites for catalytic reduction of 4-nitrophenol. *J. Colloid Interface Sci.* **2014**, *423*, 54–59. [CrossRef]

9. Lv, W.; Wang, Y.; Feng, W.; Qi, J.; Zhang, G.; Zhang, F.; Fan, X. Robust and smart gold nanoparticles: One-step synthesis, tunable optical property, and switchable catalytic activity. *J. Mater. Chem.* **2011**, *21*, 6173–6178. [CrossRef]

10. Sardar, R.; Funston, A.M.; Mulvaney, P.; Murray, R.W. Gold nanoparticles: Past, present, and future. *Langmuir* **2009**, *25*, 13840–13851. [CrossRef] [PubMed]

11. Zhang, P.; Shao, C.; Zhang, Z.; Zhang, M.; Mu, J.; Guo, Z.; Liu, Y. In situ assembly of well-dispersed Ag nanoparticles (AgNPs) on electrospun carbon nanofibers (CNFs) for catalytic reduction of 4-nitrophenol. *Nanoscale* **2011**, *3*, 3357–3363. [CrossRef] [PubMed]

12. Zhang, Z.; Shao, C.; Sun, Y.; Mu, J.; Zhang, M.; Zhang, P.; Guo, Z.; Liang, P.; Wang, C.; Liu, Y. Tubular nanocomposite catalysts based on size-controlled and highly dispersed silver nanoparticles assembled on electrospun silica nanotubes for catalytic reduction of 4-nitrophenol. *J. Mater. Chem.* **2012**, *22*, 1387–1395. [CrossRef]

13. Hsu, K.C.; Chen, D.H. Green synthesis and synergistic catalytic effect ofAg/reduced graphene oxide nanocomposite. *Nanoscale Res. Lett.* **2014**, *9*, 484. [CrossRef] [PubMed]

14. Chiou, J.R.; Lai, B.H.; Hsu, K.C.; Chen, D.H. One-pot green synthesis of silver/iron oxide composite nanoparticles for 4-nitrophenol reduction. *J. Hazard. Mater.* **2013**, *248–249*, 394–400. [CrossRef] [PubMed]

15. Huang, S.; Xiao, Z.; Zhai, S.; Zhai, B.; Zhang, F.; An, Q. Fabrication of highly-stable Ag/CA@GTA hydrogel beads and their catalytic application. *RSC Adv.* **2014**, *4*, 60460–60466. [CrossRef]

16. Özkar, S.; Finke, R.G. Nanocluster formation and stabilization fundamental studies: Ranking commonly employed anionic stabilizers via the development, then application, of five comparative criteria. *J. Am. Chem. Soc.* **2002**, *124*, 5796–5810. [CrossRef] [PubMed]

17. Saha, S.; Pal, A.; Kundu, S.; Basu, S.; Pal, T. Photochemical green synthesis of calcium-alginate-stabilized ag and au nanoparticles and their catalytic application to 4-nitrophenol reduction. *Langmuir* **2010**, *26*, 2885–2893. [CrossRef] [PubMed]

18. Hortigüela, M.J.; Aranaz, I.; Gutiérrez, M.C.; Ferrer, M.L.; Del Monte, F. Chitosan gelation induced by the in situ formation of gold nanoparticles and its processing into macroporous scaffolds. *Biomacromolecules* **2011**, *12*, 179–186. [CrossRef] [PubMed]

19. Chtchigrovsky, M.; Lin, Y.; Ouchaou, K.; Chaumontet, M.; Robitzer, M.; Quignard, F.; Taran, F. Dramatic effect of the gelling cation on the catalytic performances of alginate-supported palladium nanoparticles for the Suzuki-Miyaura reaction. *Chem. Mater.* **2012**, *24*, 1505–1510. [CrossRef]

20. Khan, M.Z.; Ashraf, M.; Hussain, T.; Rehman, A.; Malik, M.M.; Raza, Z.A.; Nawab, Y.; Zia, Q. In situ deposition of TiO2 nanoparticles on polyester fabric and study of its functional properties. *Fibers Polym.* **2015**, *16*, 1092–1097. [CrossRef]

21. Babaahmadi, V.; Montazer, M. Reduced graphene oxide/SnO2 nanocomposite on PET surface: Synthesis, characterization and application as an electro-conductive and ultraviolet blocking textile. *Colloids Surfaces A Physicochem. Eng. Asp.* **2016**, *506*, 507–513. [CrossRef]

22. Mohammadi, M.; Karimi, L.; Mirjalili, M. Simultaneous synthesis of nano ZnO and surface modification of polyester fabric. *Fibers Polym.* **2016**, *17*, 1371–1377. [CrossRef]

23. Guo, M.X.; Bian, S.W.; Shao, F.; Liu, S.; Peng, Y.H. Hydrothermal synthesis and electrochemical performance of MnO2/graphene/polyester composite electrode materials for flexible supercapacitors. *Electrochim. Acta* **2016**, *209*, 486–497. [CrossRef]

24. Karimi, L.; Yazdanshenas, M.E.; Khajavi, R.; Rashidi, A.; Mirjalili, M. Optimizing the photocatalytic properties and the synergistic effects of graphene and nano titanium dioxide immobilized on cotton fabric. *Appl. Surf. Sci.* **2015**, *332*, 665–673. [CrossRef]

25. Tian, M.; Tang, X.; Qu, L.; Zhu, S.; Guo, X.; Han, G. Robust ultraviolet blocking cotton fabric modified with chitosan/graphene nanocomposites. *Mater. Lett.* **2015**, *145*, 340–343. [CrossRef]

26. Moazami, A.; Montazer, M.; Dolatabadi, M.K. Reduction of 4-nitrophenol to 4-aminophenol over sonoimmobilized silver/reduced graphene oxide nanocomposites on polyester fabric. *Fibers Polym.* **2017**, *18*, 2287–2297. [CrossRef]

27. Lee, M.S.; Lee, M.; Wakida, T.; Saito, M.; Yamashiro, T.; Nishi, K.; Inoue, G.; Ishida, S. Ozone-gas treatment of cationic dyeable polyester and poly(butylene terephthalate) fibers. *J. Appl. Polym. Sci.* **2007**, *104*, 2423–2429. [CrossRef]

28. Moazami, A.; Montazer, M.; Dolatabadi, M.K. Tunable functional properties on polyester fabric using simultaneous green reduction of graphene oxide and silver nitrate. *Fibers Polym.* **2016**, *17*, 1359–1370. [CrossRef]

29. Majdoub, M.; Amedlous, A.; Anfar, Z.; Jada, A.; El Alem, N. Engineering of amine-based binding chemistry on functionalized graphene oxide/alginate hybrids for simultaneous and efficient removal of trace heavy metals: Towards drinking water. *J. Colloid Interface Sci.* **2021**, *589*, 511–524. [CrossRef] [PubMed]

30. Tu, W.; Zhou, Y.; Zou, Z. Versatile graphene-promoting photocatalytic performance of semiconductors: Basic principles, synthesis, solar energy conversion, and environmental applications. *Adv. Funct. Mater.* **2013**, *23*, 4996–5008. [CrossRef]

31. Wang, Y.; Shi, R.; Lin, J.; Zhu, Y. Enhancement of photocurrent and photocatalytic activity of ZnO hybridized with graphite-like C3N4. *Energy Environ. Sci.* **2011**, *4*, 2922–2929. [CrossRef]

32. Li, X.; Li, M.; Yang, J.; Li, X.; Hu, T.; Wang, J.; Sui, Y.; Wu, X.; Kong, L. Synergistic effect of efficient adsorption g-C3N4/ZnO composite for photocatalytic property. *J. Phys. Chem. Solids* **2014**, *75*, 441–446. [CrossRef]

33. Pan, C.; Xu, J.; Wang, Y.; Li, D.; Zhu, Y. Dramatic activity of C 3N 4/BiPO 4 photocatalyst with core/shell structure formed by self-assembly. *Adv. Funct. Mater.* **2012**, *22*, 1518–1524. [CrossRef]

34. Lv, H.; Ji, G.; Yang, Z.; Liu, Y.; Zhang, X.; Liu, W.; Zhang, H. Enhancement photocatalytic activity of the graphite-like C3N4 coated hollow pencil-like ZnO. *J. Colloid Interface Sci.* **2015**, *450*, 381–387. [CrossRef] [PubMed]

35. Tian, K.; Liu, W.J.; Jiang, H. Comparative investigation on photoreactivity and mechanism of biogenic and chemosythetic Ag/C3N4 composites under visible light irradiation. *ACS Sustain. Chem. Eng.* **2015**, *3*, 269–276. [CrossRef]

36. Majdoub, M.; Amedlous, A.; Anfar, Z.; Moussaoui, O. MoS2 nanosheets/silver nanoparticles anchored onto textile fabric as "dip catalyst" for synergistic p-nitrophenol hydrogenation. *Environ. Sci. Pollut. Res.* **2021**, *28*, 64674–64686. [CrossRef] [PubMed]

37. Yang, S.; Gong, Y.; Zhang, J.; Zhan, L.; Ma, L.; Fang, Z.; Vajtai, R.; Wang, X.; Ajayan, P.M. Exfoliated Graphitic Carbon Nitride Nanosheets as Efficient Catalysts for Hydrogen Evolution Under Visible Light. *Adv. Mater.* **2013**, *25*, 2452–2456. [CrossRef]

38. Ding, X.; Zhu, J.; Zhang, Y.; Xia, Q.; Bi, W.; Yang, X.; Yang, J. Separation and concentration of natural products by fast forced adsorption using well-dispersed velvet-like graphitic carbon nitride with response surface methodology optimisation. *Talanta* **2016**, *154*, 119–126. [CrossRef]

39. Zhang, S.; Gao, H.; Huang, Y.; Wang, X.; Hayat, T.; Li, J.; Xu, X.; Wang, X. Ultrathin g-C3N4 nanosheets coupled with amorphous Cu-doped FeOOH nanoclusters as 2D/0D heterogeneous catalysts for water remediation. *Environ. Sci. Nano* **2018**, *5*, 1179–1190. [CrossRef]

40. Wang, Z.; Guan, W.; Sun, Y.; Dong, F.; Zhou, Y.; Ho, W.K. Water-assisted production of honeycomb-like g-C3N4with ultralong carrier lifetime and outstanding photocatalytic activity. *Nanoscale* **2015**, *7*, 2471–2479. [CrossRef]

41. Majdoub, M.; Anfar, Z.; Amedlous, A. Emerging Chemical Functionalization of g-C3N4: Covalent/Noncovalent Modifications and Applications. *ACS Nano* **2020**, *14*, 12390–12469. [CrossRef]

42. Zhao, S.; Zhao, X.; Ouyang, S.; Zhu, Y. Polyoxometalates covalently combined with graphitic carbon nitride for photocatalytic hydrogen peroxide production. *Catal. Sci. Technol.* **2018**, *8*, 1686–1695. [CrossRef]

43. Jürgens, B.; Irran, E.; Senker, J.; Kroll, P.; Müller, H.; Schnick, W. Melem (2,5,8-Triamino-tri- *s* -triazine), an Important Intermediate during Condensation of Melamine Rings to Graphitic Carbon Nitride: Synthesis, Structure Determination by X-ray Powder Diffractometry, Solid-State NMR, and Theoretical Studies. *J. Am. Chem. Soc.* **2003**, *125*, 10288–10300. [CrossRef]

44. Xu, J.; Shang, J.K.; Jiang, Q.; Wang, Y.; Li, Y.X. Facile alkali-assisted synthesis of g-C3N4 materials and their high-performance catalytic application in solvent-free cycloaddition of CO2 to epoxides. *RSC Adv.* **2016**, *6*, 55382–55392. [CrossRef]

45. Molina, J.; Zille, A.; Fernández, J.; Souto, A.P.; Bonastre, J.; Cases, F. Conducting fabrics of polyester coated with polypyrrole and doped with graphene oxide. *Synth. Met.* **2015**, *204*, 110–121. [CrossRef]

46. Berendjchi, A.; Khajavi, R.; Yousefi, A.A.; Yazdanshenas, M.E. Improved continuity of reduced graphene oxide on polyester fabric by use of polypyrrole to achieve a highly electro-conductive and flexible substrate. *Appl. Surf. Sci.* **2016**, *363*, 264–272. [CrossRef]

47. Alongi, J.; Camino, G.; Malucelli, G. Heating rate effect on char yield from cotton, poly(ethylene terephthalate) and blend fabrics. *Carbohydr. Polym.* **2013**, *92*, 1327–1334. [CrossRef] [PubMed]

48. Yu, W.; Xu, D.; Peng, T. Enhanced photocatalytic activity of g-C3N4 for selective CO2 reduction to CH3OH via facile coupling of ZnO: A direct Z-scheme mechanism. *J. Mater. Chem. A* **2015**, *3*, 19936–19947. [CrossRef]

49. Hou, S.; Li, J.; Huang, X.; Wang, X.; Ma, L.; Shen, W.; Kang, F.; Huang, Z.-H. Silver Nanoparticles-Loaded Exfoliated Graphite and Its Anti-Bacterial Performance. *Appl. Sci.* **2017**, *7*, 852. [CrossRef]

50. Dakal, T.C.; Kumar, A.; Majumdar, R.S.; Yadav, V. Mechanistic basis of antimicrobial actions of silver nanoparticles. *Front. Microbiol.* **2016**, *7*, 1831. [CrossRef]

51. Gangula, A.; Podila, R.; Karanam, L.; Janardhana, C.; Rao, A.M. Catalytic reduction of 4-nitrophenol using biogenic gold and silver nanoparticles derived from breynia rhamnoides. *Langmuir* **2011**, *27*, 15268–15274. [CrossRef] [PubMed]

52. Chang, G.; Luo, Y.; Lu, W.; Qin, X.; Asiri, A.M.; Al-Youbi, A.O.; Sun, X. Ag nanoparticles decorated polyaniline nanofibers: Synthesis, characterization, and applications toward catalytic reduction of 4-nitrophenol and electrochemical detection of H2O2 and glucose. *Catal. Sci. Technol.* **2012**, *2*, 800–806. [CrossRef]

53. Tian, Y.; Cao, Y.Y.; Pang, F.; Chen, G.Q.; Zhang, X. Ag nanoparticles supported on N-doped graphene hybrids for catalytic reduction of 4-nitrophenol. *RSC Adv.* **2014**, *4*, 43204–43211. [CrossRef]

54. Qiao, X.Q.; Zhang, Z.W.; Tian, F.Y.; Hou, D.F.; Tian, Z.F.; Li, D.S.; Zhang, Q. Enhanced Catalytic Reduction of p-Nitrophenol on Ultrathin MoS2 Nanosheets Decorated with Noble Metal Nanoparticles. *Cryst. Growth Des.* **2017**, *17*, 3538–3547. [CrossRef]

55. Wang, M.; Tian, D.; Tian, P.; Yuan, L. Synthesis of micron-SiO2 @nano-Ag particles and their catalytic performance in 4-nitrophenol reduction. *Appl. Surf. Sci.* **2013**, *283*, 389–395. [CrossRef]

56. Du, X.; He, J.; Zhu, J.; Sun, L.; An, S. Ag-deposited silica-coated Fe3O4 magnetic nanoparticles catalyzed reduction of p-nitrophenol. *Appl. Surf. Sci.* **2012**, *258*, 2717–2723. [CrossRef]

57. Ayodhya, D.; Veerabhadram, G. Synthesis and characterization of g-C3N4 nanosheets decorated Ag2S composites for investigation of catalytic reduction of 4-nitrophenol, antioxidant and antimicrobial activities. *J. Mol. Struct.* **2019**, *1186*, 423–433. [CrossRef]

58. Baruah, B.; Gabriel, G.J.; Akbashev, M.J.; Booher, M.E. Facile synthesis of silver nanoparticles stabilized by cationic polynorbornenes and their catalytic activity in 4-nitrophenol reduction. *Langmuir* **2013**, *29*, 4225–4234. [CrossRef] [PubMed]

59. Gu, S.; Wunder, S.; Lu, Y.; Ballauff, M.; Fenger, R.; Rademann, K.; Jaquet, B.; Zaccone, A. Kinetic analysis of the catalytic reduction of 4-nitrophenol by metallic nanoparticles. *J. Phys. Chem. C* **2014**, *118*, 18618–18625. [CrossRef]

60. Amedlous, A.; Majdoub, M.; Amaterz, E.; Anfar, Z.; Benlhachemi, A. Synergistic Effect of g-C3N4 Nanosheets/Ag3PO4 Microcubes as Efficient n-p-Type Heterostructure based Photoanode for Photoelectrocatalytic Dye Degradation. *J. Photochem. Photobiol. A Chem.* **2021**, 113127. [CrossRef]

61. Lee, D.T.; Zhao, J.; Peterson, G.W.; Parsons, G.N. Catalytic "mOF-Cloth" Formed via Directed Supramolecular Assembly of UiO-66-NH2 Crystals on Atomic Layer Deposition-Coated Textiles for Rapid Degradation of Chemical Warfare Agent Simulants. *Chem. Mater.* **2017**, *29*, 4894–4903. [CrossRef]